

# Energy-Driven Adaptive Visual Token Pruning for Efficient Vision-Language Models

Jialuo He<sup>1</sup> and Huangxun Chen<sup>1</sup>

The Hong Kong University of Science and Technology (Guangzhou)  
huangxunchen@hkust-gz.edu.cn

**Abstract.** Visual token reduction is critical for accelerating Vision-Language Models (VLMs), yet most existing approaches rely on a fixed budget shared across all inputs, overlooking the substantial variation in image information density. We propose E-AdaPrune, an energy-driven adaptive pruning framework that determines the token budget from the singular value spectrum of the visual features space. By preserving a certain proportion of spectral energy, our method allocates more tokens to information-dense scenes while aggressively compressing redundant ones, without introducing additional learnable parameters. We evaluate E-AdaPrune on nine benchmarks and three VLM backbones, LLaVA-1.5-7B, LLaVA-1.5-13B, and LLaVA-NeXT-8B. Under matched average token budgets, E-AdaPrune consistently yields an average improvement of up to 0.6%, including a significant +5.1% relative boost on the MMVet reasoning task. Using randomized singular value decomposition, the additional latency is limited to 8ms per image.

**Keywords:** Efficient Vision-Language Models · Adaptive Pruning

## 1 Introduction

Large Vision-Language Models (LVLMs) [3, 9, 11, 18, 23–26, 31, 34, 36, 46, 49] have demonstrated exceptional capabilities across diverse multimodal tasks, including complex visual reasoning, fine-grained instruction following, and document understanding [17, 20, 33]. To capture the necessary semantic depth, these models represent visual inputs as high-resolution sequences of tokens. However, this high-resolution representation introduces significant computational overhead, primarily due to the quadratic complexity of the self-attention mechanism within the Large Language Model (LLM) backbone [21, 35, 41, 45]. Empirical evidence suggests that visual tokens inherently contain substantial redundancy, with only a small fraction of tokens being essential for accurate response generation [5, 8, 18, 43].

To address this inefficiency, existing literature has explored visual token pruning strategies, which can be categorized into feature abstraction [10, 18, 49], token merging [7, 14, 32], and token dropping [8, 37, 38, 47]. While these methods effectively reduce the sequence length, they predominantly rely on a "one-size-fits-all"



**Fig. 1:** Different images contain different amounts of visual information, indicating that a static token budget may either discard critical details or retain unnecessary redundancy. All examples are from TextVQA [33].

strategy, utilizing a fixed top- $k$  budget or a predefined pruning ratio across all input instances. Such static approaches fail to account for the significant variability in information density between different images. For example, as shown in Fig. 1, in an information-dense scene like a crowded bar containing numerous legible labels, a model might require more tokens to correctly identify a specific brand, whereas a simple scene with a few mobile phones can be accurately processed with fewer tokens. Applying a static budget, such as the  $k$ -token mean used in some baselines, leads to over-pruning in complex scenes, causing information loss, and under-pruning in simple scenes, wasting computational resources.

To overcome these limitations, recent research has explored adaptive token reduction mechanisms that modulate visual token length. Methods such as ATP-LLaVA [42] utilize learnable thresholds for instance-specific pruning ratios, while VCM [29] extracts task-relevant concepts via optimization procedures. Vision-Think [39] further employs reinforcement learning to determine whether higher-resolution inputs are required. However, these approaches typically require additional training or policy optimization to enable dynamic behavior.

In this paper, we propose E-AdaPrune, a training-free and plug-and-play Energy-driven Adaptive Pruning framework. We argue that the appropriate token budget is an intrinsic property of the image representation rather than a fixed heuristic. Different images induce visual feature matrices with distinct spectral structures, reflecting variations in semantic density and redundancy. Based on this observation, E-AdaPrune estimates the minimal token budget by analyzing the singular value spectrum of the visual feature matrix and preserving a certain proportion of spectral energy.

Importantly, E-AdaPrune introduces no new learnable parameters and decouples budget estimation from token selection, making it model-agnostic and orthogonal to existing pruning strategies [8, 37, 38]. It can therefore be seamlessly integrated into existing pruning pipelines without modification, and can generalize across architectures.

Our contributions are summarized as follows:

- We reformulate visual token budgeting as an intrinsic spectral property of the image feature space and propose an energy-based adaptive criterion for content-aware compression.
- We design a training-free, plug-and-play module that integrates with existing pruning strategies without modifying their scoring mechanisms.
- Across three LVLm backbones and nine benchmarks, E-AdaPrune consistently yields an average performance improvement of up to 0.6%, highlighted by a +5.1% relative gain over static baselines on the MMVet benchmark, while incurring only 8ms of additional latency via randomized Singular Value Decomposition (rSVD).

## 2 Related Work

This section situates E-AdaPrune within the evolving landscape of efficient Vision-Language Models by categorizing existing literature based on the mechanism of visual information reduction. We first examine the theoretical and empirical foundations of visual token redundancy, which justify the feasibility of compression. We then analyze static Top- $k$  pruning strategies that utilize fixed budget constraints. Finally, we discuss the recent shift toward adaptive pruning frameworks that dynamically modulate token density, providing the necessary context for our proposed energy-driven selection mechanism.

### 2.1 Visual Token Redundancy in LVLms

LVLms have achieved unprecedented success across a broad spectrum of multimodal applications, ranging from complex visual reasoning to fine-grained instruction following [2, 3, 10, 18, 24–26, 31, 36, 46]. To capture intricate details, these models typically represent visual inputs as an extensive sequence of tokens. However, this high-resolution representation inherently introduces substantial visual redundancy, as visual patches often contain vast amounts of task-irrelevant background information.

Empirical studies have shown that only a small fraction of these tokens are essential for the model to generate accurate responses [5, 8, 16, 19, 22, 29, 37–39, 42, 43, 47, 48, 50]. The presence of such redundancy leads to two consequences: it imposes a heavy computational burden and excessive memory consumption, particularly due to the quadratic complexity of the self-attention mechanism in the LLM backbone [41, 45].

### 2.2 Fixed-Budget Token Reduction

Existing visual token compression methods can be broadly categorized into feature abstraction, token merging, and token dropping. Feature abstraction methods resample visual features into a fixed number of latent tokens using learnable query-based bottlenecks, producing constant-length representations independent of input resolution, as exemplified by BLIP-2 [18], InstructBLIP [10],

and MiniGPT-4 [1]. Token merging methods reduce token cardinality by aggregating similar patches into representative embeddings based on similarity metrics or hierarchical grouping [4, 7, 14, 32, 40].

Token dropping methods instead discard uninformative tokens to accelerate inference. Prior work estimates token importance using cross-modal or self-attention scores [6, 8, 48] or pure vision signals [38, 47]; progressively increases sparsity across layers [37]. Although these approaches differ in scoring mechanisms and pruning locations, most of them adopt a fixed top- $k$  or predefined pruning ratio shared across all inputs, thereby ignoring the variability of information density across images.

To address this limitation, we propose E-AdaPrune, which determines the token budget  $k^*$  using an image-specific energy criterion, enabling content-aware compression while remaining compatible with existing dropping heuristics.

## 2.3 Adaptive Reduction

To overcome the limitations of fixed budgets, recent work has explored adaptive token reduction mechanisms. ATP-LLaVA [42] introduces learnable thresholds to determine instance-specific and layer-wise pruning ratios through an Adaptive Token Pruning module. VCM [29] formulates adaptive compression as a vision concept modeling problem, dynamically extracting task-relevant concepts via a forward-backward optimization procedure. VisionThink [39] further employs reinforcement learning to decide whether low-resolution inputs suffice or higher-resolution images are necessary for reasoning.

However, these adaptive methods typically rely on additional training to enable dynamic behavior. In contrast, E-AdaPrune is training-free and requires no extra learnable parameters. Furthermore, E-AdaPrune is orthogonal to existing pruning methods. By decoupling budget determination from token selection, it can be integrated with methods such as FastV [8], PyramidDrop [37], and VisionZip [38] without modifying their internal mechanisms, enabling adaptive compression within existing acceleration pipelines.

# 3 Method

In this section, we present E-AdaPrune, an energy-driven adaptive pruning framework. We begin by establishing the preliminaries of Vision-Language Models (VLMs) and the traditional "one-size-fits-all" token dropping paradigm. We then demonstrate the architectural flexibility of our approach, which allows for seamless integration with existing pruning heuristics. Finally, we provide the formal technical derivation of E-AdaPrune.

## 3.1 Preliminaries

**Vision-Language Models.** Modern VLMs typically consist of three core components: a vision encoder  $\mathcal{E}_V$ , a projector  $\mathcal{P}$ , and an LLM  $\mathcal{L}$  [2, 18, 24–26]. The

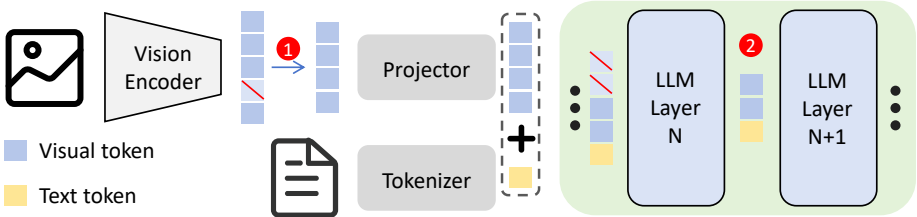


**Fig. 2:** VLM forward process architecture. Circled numbers indicate viable locations for visual token pruning: ① the vision-LLM interface and ② intermediate LLM layers.

vision encoder  $\mathcal{E}_V$  maps an input image  $\mathcal{X}^V$  into a visual feature space:

$$\mathbf{Z}^V = \mathcal{E}_V(\mathcal{X}^V) \in \mathbb{R}^{n_v \times d_v}, \quad (1)$$

where  $n_v$  and  $d_v$  denote the number of output visual tokens and their respective feature dimensions. Subsequently, the projector  $\mathcal{P}$  aligns these visual tokens into the text embedding space:

$$\mathbf{H}^V = \mathcal{P}(\mathbf{Z}^V) \in \mathbb{R}^{n_v \times d_t}, \quad (2)$$

where  $d_t$  is the text hidden dimension. The LLM, composed of a text encoder  $\mathcal{E}_t$  and an  $M$ -layer Transformer decoder  $F$ , processes the concatenated visual and textual features:

$$\mathbf{Y} = F[\mathbf{H}^V; \mathcal{E}_t(\mathcal{X}^T)]. \quad (3)$$

Here,  $\mathcal{X}^T$  represents the input text, including system prompts, user queries, and dialogue history, while  $[\cdot; \cdot]$  denotes the concatenation operation and  $\mathbf{Y}$  is the generated output sequence.

Since the computational complexity of the self-attention mechanism grows quadratically with the sequence length, the high-resolution representation  $n_v$  remains a primary efficiency bottleneck.

**Visual Token Redundancy.** To mitigate the computational costs of long visual sequences, pruning can be executed at the vision-LLM interface or during LLM prefilling. Current methods typically assign importance scores via heuristics, such as attention weights or feature norms, to identify and discard redundant tokens. However, as illustrated in Fig. 2, these "one-size-fits-all" strategies employ a static budget  $k$  that ignores the inherent variability of information density across images, as shown in Fig. 3. Consequently, static pruning often leads to over-pruning in complex, information-dense scenes, e.g., dense text, or resource wastage in simple ones.

### 3.2 E-AdaPrune: Energy-Based Adaptive Pruning

The fundamental premise of E-AdaPrune is that visual information density varies significantly across different images, a property we term image energy. While

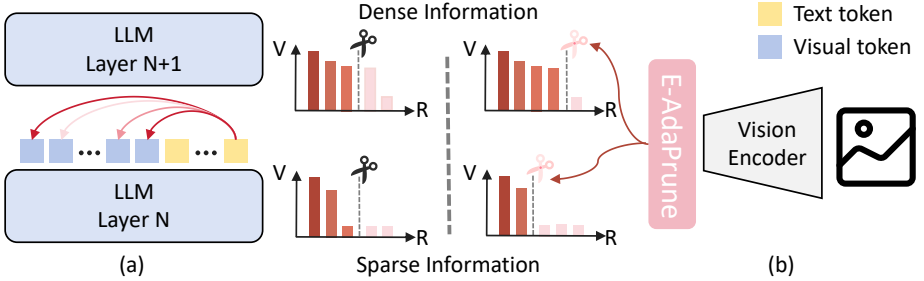


**Fig. 3:** Comparison of static and adaptive pruning. (a) FastV uses a fixed top- $k$  budget regardless of image content. (b) E-AdaPrune determines a content-aware budget  $k^*$  via an image-specific energy criterion, optimizing token retention for varying information densities.  $V$  and  $R$  denote token importance scores and rankings.

existing research suggests that specific tasks like document understanding or high-precision Optical Character Recognition (OCR) necessitate a larger or even full token budget [19], we argue that this requirement is an intrinsic property of the image feature space rather than a task-specific heuristic.

To implement this observation, we decouple the visual compression process into an energy-based budget determination phase and a subsequent selection phase. This decoupling provides two distinct architectural benefits. First, it ensures seamless compatibility with diverse top- $k$  selection heuristics by substituting a static budget with a dynamic, image-specific  $k^*$ . Second, by relying exclusively on the intrinsic spectral properties of the visual features, our approach is inherently text-agnostic. This design choice avoids the potential vulnerabilities associated with text-dependent pruning, which literature has shown can suffer from performance instability in scenarios where the visual importance is overly specialized to a specific prompt [16].

**Singular Value Decomposition of  $\mathbf{Z}^V$ .** By grounding the compression budget in the feature matrix  $\mathbf{Z}^V$  itself, we ensure that the information retention remains robust regardless of the complexity or length of the accompanying text query. We formalize this by treating the visual feature matrix  $\mathbf{Z}^V \in \mathbb{R}^{n_v \times d_v}$  as a signal-carrying entity, allowing us to quantify its information content through spectral energy distribution. We apply Singular Value Decomposition (SVD) to the visual features such that:

$$(\mathbf{U}, \mathbf{S}, \mathbf{V}^\top) = \text{SVD}(\mathbf{Z}^V), \quad (4)$$

where the singular values  $\sigma = \text{diag}(\mathbf{S})$  represent the variance captured along each principal component. Since each squared singular value  $\sigma_i^2$  represents the variance or energy captured by its corresponding principal component, the total energy of the feature space is equivalent to the sum of the squared singular

---

**Algorithm 1:** Energy-based Adaptive Rank Selection
 

---

**Input:** Visual features  $\mathbf{Z}^V \in \mathbb{R}^{n_v \times d_v}$ , Energy threshold  $\tau$ , Min rank  $k_{min}$ ,  
 Max rank  $k_{max}$

**Output:** Optimal rank  $k^*$ , Dropping ratio  $\rho$

```

1 ( $\mathbf{U}, \mathbf{S}, \mathbf{V}^\top$ )  $\leftarrow$  SVD( $\mathbf{Z}^V$ ); // Singular Value Decomposition
2  $\sigma \leftarrow \text{diag}(\mathbf{S})$ ; // Vector of singular values
3  $e_i \leftarrow \sigma_i^2$ ; // Energy of the  $i$ -th component
4  $E_{total} \leftarrow \sum_{j=1}^{\min(n_v, d_v)} e_j$ ;
5 for  $k = 1$  to  $\min(n_v, d_v)$  do
6    $C(k) \leftarrow \frac{\sum_{i=1}^k e_i}{E_{total}}$ ; // Cumulative energy ratio
7   if  $C(k) \geq \tau$  then
8      $k_{raw} \leftarrow k$ ;
9     break;
10  $k^* \leftarrow \max(k_{min}, \min(k_{raw}, k_{max}))$ ;
11  $\rho \leftarrow 1 - k^*/k_{max}$ ;
12 return  $k^*, \rho$ 

```

---

values:

$$E_{total} = \sum_{i=1}^n \sigma_i^2, \quad (5)$$

where  $n = \min(n_v, d_v)$  is the total number of singular values.

This energy decomposition allows us to analyze the information density of an image through the lens of spectral concentration. Images with high redundancy exhibit a steep spectral decay, where a few components dominate the total energy, whereas complex scenes with dense information yield a flatter spectrum, indicating that information is dispersed across a wider range of components.

The rate of spectral decay provides a quantitative measure of image-specific information density. To effectively utilize this property, we introduce an energy preservation criterion that serves as an information floor for the pruning process. To ensure that the pruned visual sequence maintains sufficient semantic integrity for complex reasoning, we define a preservation target,  $\tau$ , which represents the cumulative fraction of the total energy that must be retained.

This threshold acts as a safeguard; in images where the spectrum is flat, the energy is distributed across many components, requiring a larger subset to satisfy the target. Conversely, in redundant scenes where the energy is concentrated in a few dominant components, the target is met with a significantly smaller budget. The adaptive relationship between image complexity and its spectral energy distribution is visualized in Fig. 4, where the adaptive rank  $k^*$  is determined by the cumulative energy preservation threshold  $\tau$ .

To bridge the gap between this theoretical energy analysis and a practical inference budget, we first determine the raw adaptive rank  $k_{raw}$  as the minimum number of components necessary to meet or exceed the energy preservation

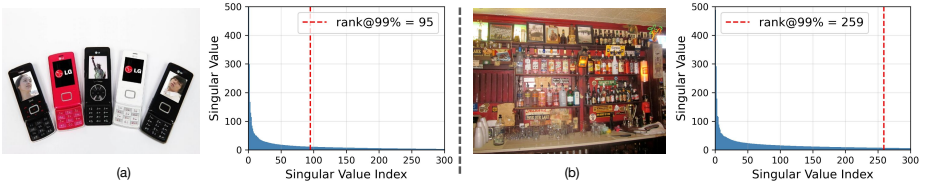


**Fig. 4:** Singular value spectra comparison. Simple image (a) shows sharp decay with  $k^* = 95$ . Hard image (b) has a flat spectrum requiring  $k^* = 259$ . Red dashed lines indicate the adaptive rank at  $\tau = 99\%$ .

threshold  $\tau$ :

$$k_{raw} = \min \left\{ k \in \{1, \dots, n\} \mid \frac{\sum_{i=1}^k \sigma_i^2}{\sum_{i=1}^n \sigma_i^2} \geq \tau \right\} \quad (6)$$

While  $k_{raw}$  represents the ideal information-centric budget, practical deployment requires reasonable boundary constraints to maintain stability within the LLM. Thus, the finalized optimal rank  $k^*$  is obtained by clamping  $k_{raw}$  between a predefined minimum  $k_{min}$  and maximum  $k_{max}$ , as detailed in Algorithm 1.

This adaptive mechanism is illustrated in Fig. 3, where we contrast our approach with the static paradigm of FastV [8]. Unlike static methods that fix a budget  $k$  regardless of content, E-AdaPrune dynamically modulates the pruning ratio  $\rho$  based on the input’s intrinsic energy. In this framework,  $\tau$  functions as a global hyperparameter that guarantees a consistent level of information preservation across heterogeneous datasets, while the actual number of tokens  $k^*$  adapts to the complexity of each input instance. Once  $k^*$  is calculated, it serves as the dynamic cut-off point for the importance rankings provided by the integrated selection heuristic. For instance, when combined with FastV [8],  $k^*$  replaces the static  $k$  to truncate tokens based on attention scores, while in the context of VisionZip [38], it adaptively modulates the number of dominant tokens based on the observed spectral decay.

**Randomized SVD.** Despite the adaptive benefits of spectral analysis, performing a full SVD on the visual feature matrix  $\mathbf{Z}^V \in \mathbb{R}^{n_v \times d_v}$  introduces significant computational overhead. Specifically, the exact SVD requires  $O(n_v d_v \min(n_v, d_v))$  operations, which may offset the latency gains achieved through token pruning.

To mitigate this, we employ rSVD [13, 30]. Instead of decomposing the entire matrix, we first project  $\mathbf{Z}^V$  onto a smaller, random subspace to identify its most significant range. We then perform the decomposition on this compressed representation. This approach captures the essential singular value spectrum with high probability while avoiding the cost of a full matrix factorization.

By utilizing a random projection matrix to approximate the range of the feature matrix, we reduce the theoretical complexity to  $O(n_v d_v t + t^2 d_v)$ , where  $t$  is the target rank. As detailed in Appendix: Algorithm 2, this randomized approximation allows E-AdaPrune to remain a lightweight, plug-and-play module that

provides content-aware adaptivity with negligible impact on the overall inference pipeline.

## 4 Experiment

In this section, we evaluate the performance and efficiency of E-AdaPrune. We first establish the experimental setup by calibrating adaptive token budgets against static baselines across multiple benchmarks. We then present the main results on LLaVA-1.5-7B, followed by a scaling analysis on larger model architectures. Finally, we provide a detailed overhead analysis to evaluate computational efficiency.

### 4.1 Experiment Setup

**Datasets.** We conduct evaluations on a broad range of benchmarks to ensure comprehensive coverage of VLM capabilities, including GQA [15], MMBench (MMB) [27], MME [12], POPE [20], SQA [28], SEED-Bench (SEED) [17], VQA-Text (TextVQA) [33], and MMVet [44].

**Models** Our framework is applied to several architectures, including LLaVA-1.5-7B, LLaVA-1.5-13B [26], and LLaVA-NeXT-8B [25], to demonstrate its generalizability across different model sizes and families.

**Compare Baselines.** We integrate E-AdaPrune with three representative visual token pruning strategies:

- FastV [8]: A plug-and-play inference acceleration method that identifies inefficient attention in deep layers and prunes low-attention visual tokens after a specific layer.
- PyramidDrop (PDrop) [37]: A strategy that progressively reduces visual redundancy by dropping image tokens across multiple stages, maintaining full tokens in shallow layers while increasing sparsity in deeper layers.
- VisionZip [38]: A text-agnostic pruning approach that selects dominant informative tokens and merges the remaining contextual tokens based on semantic similarity before feeding them into the LLM.

**Implementation Details.** To facilitate a fair comparison between our adaptive framework and static baseline methods, we first calibrate the token budgets. For each benchmark, we apply an energy threshold of  $\tau = 99.8\%$  or  $\tau = 99.0\%$  to the input images to determine the specific number of effective visual tokens required for each instance. Based on these measurements, we calculate the mean effective token count across the dataset. This mean value is then utilized as the fixed budget  $k$  for the static baselines, ensuring that both adaptive and static strategies operate at the same average computational cost.

Regarding implementation, we adhere to the default configurations of the baseline models except for the budget selection. For FastV [8], visual tokens are pruned after layer 2, corresponding to  $K = 2$ . In the case of PDrop [37], we utilize a pruning layer list of [8, 16, 24] and apply clamping to the dropping ratio  $\rho$  to ensure stability. Specifically,  $\rho$  is constrained to the interval [0.4, 0.6] for  $\tau = 99.8\%$  and to [0.6, 0.8] for  $\tau = 99.0\%$ . For VisionZip [38], the number of contextual tokens is fixed at 30 across all experimental evaluations.

## 4.2 Main Results.

**Results of LLaVA-1.5-7B.** As illustrated in Table 1, the integration of E-AdaPrune, which is denoted as "+E", consistently improves the average performance of all baseline methods. E-AdaPrune achieves a 5.1% relative boost on MMVet, 107.7% vs. 102.6% for PDrop. MMVet requires fine-grained reasoning for information-dense scenes, where static budgets often discard critical tokens. By identifying flat spectra, E-AdaPrune adaptively preserves more essential semantic cues for complex understanding.

A critical observation from our results is the relationship between the energy preservation target  $\tau$  and the resulting performance gain. When the target is high, such as  $\tau = 99.8\%$ , "+E" improves the average performance of FastV, PDrop, and VisionZip by 0.6%, 0.6%, and 0.5%, respectively. However, at a more aggressive compression level, when  $\tau = 99.0\%$ , the performance improvements diminish to 0.3%, 0.1%, and 0.1%.

This trend suggests that as the overall energy threshold decreases, the distribution of effective visual tokens shifts downward. In such highly constrained scenarios, the total token budget may fall below the critical threshold required for specific QA tasks, even with adaptive selection. Consequently, the performance gap between adaptive and static strategies narrows when the available information floor is insufficient to support complex visual understanding.

**Visualization.** The qualitative results in Fig. 5 highlight the core advantage of E-AdaPrune: content-aware adaptability. In the Bar scene, which contains dense textual information, e.g., labels on bottles and signs, our method adaptively retains 259 tokens, enabling the model to correctly identify "Corona". In contrast, the static FastV prunes the sequence down to a fixed 159 tokens, losing critical semantic details and resulting in an incorrect "Bud light" response. Conversely, for the simpler Phones image, E-AdaPrune identifies high redundancy and aggressively prunes the sequence to only 95 tokens while maintaining accuracy. The static method, however, wastes computational budget by keeping 159 tokens for a scene that does not require such density.

## 4.3 E-AdaPrune with Different Models

Table 2 demonstrates that E-AdaPrune scales effectively to larger and more complex models like LLaVA-1.5-13B and LLaVA-NeXT-8B. For LLaVA-NeXT,

**Table 1:** Comparative analysis of adaptive E-AdaPrune against static pruning baselines. We evaluate performance across nine benchmarks using LLaVA-1.5-7B. "+E" denotes the inclusion of our energy-based adaptive budget. For  $\tau = 99.0\%$  and  $99.8\%$ , we report the mean effective token count per dataset. Bold values highlight the superior performance within each baseline category.

Method	MME	POPE	SQA <sup>I</sup>	VQA <sup>Text</sup>	MMVet	GQA	MMB	MMB <sup>CN</sup>	SEED	Avg.
<b>Base</b>	1510	85.9	66.8	58.2	31.1	62.0	64.3	58.3	66.1	100.0%
$\tau=99.8\%$	285	309	242	294	298	312	261	261	297	284
FastV	1507	83.0	67.7	57.9	28.9	60.4	64.0	58.3	65.4	98.5%
	99.8%	96.6%	101.3%	99.5%	92.9%	97.4%	99.5%	100.0%	98.9%	
FastV+E	1514	83.1	67.9	58.1	30.0	60.3	64.7	58.7	65.2	99.1%
	100.3%	96.7%	101.6%	99.8%	96.5%	97.3%	100.6%	100.7%	98.6%	
PDrop	1501	84.9	69.6	57.6	31.9	60.5	65.0	58.5	64.5	100.1%
	99.4%	98.8%	104.2%	99.0%	102.6%	97.6%	101.1%	100.3%	97.6%	
PDrop+E	1496	84.9	69.4	57.5	33.5	60.5	65.2	59.1	64.3	100.7%
	99.1%	98.8%	103.9%	98.8%	107.7%	97.6%	101.4%	101.4%	97.3%	
VisionZip	1475	86.4	68.6	58.0	31.1	60.8	64.0	57.4	65.2	99.5%
	97.7%	100.6%	102.7%	99.7%	100.0%	98.1%	99.5%	98.5%	98.6%	
VisionZip+E	1481	86.5	68.6	57.8	31.9	60.9	64.1	58.6	65.1	100.0%
	98.1%	100.7%	102.7%	99.3%	102.6%	98.2%	99.7%	100.5%	98.5%	
$\tau=99.0\%$	151	175	114	159	158	177	130	130	161	150
FastV	1463	76.1	67.8	57.5	28.2	57.4	63.8	57.5	62.5	95.7%
	96.9%	88.6%	101.5%	98.8%	90.7%	92.6%	99.2%	98.6%	94.6%	
FastV+E	1477	76.0	68.5	57.4	29.7	57.5	63.0	56.2	62.3	96.0%
	97.8%	88.5%	102.5%	98.6%	95.5%	92.7%	98.0%	96.4%	94.3%	
PDrop	1425	81.4	69.1	56.4	27.2	58.1	63.0	56.6	60.0	95.2%
	94.4%	94.8%	103.4%	96.9%	87.5%	93.7%	98.0%	97.1%	90.8%	
PDrop+E	1400	81.9	69.5	56.6	28.3	58.3	62.0	55.8	60.1	95.3%
	92.7%	95.3%	104.0%	97.3%	91.0%	94.0%	96.4%	95.7%	90.9%	
VisionZip	1442	85.7	68.8	57.2	31.2	59.1	62.2	56.7	63.0	97.9%
	95.5%	99.8%	103.0%	98.3%	100.3%	95.3%	96.7%	97.3%	95.3%	
VisionZip+E	1438	85.7	68.8	57.4	31.0	59.5	62.5	56.8	63.0	98.0%
	95.2%	99.8%	103.0%	98.6%	99.7%	96.0%	97.2%	97.4%	95.3%	

which utilizes a multi-scale representation, we calculate the dropping ratio  $\rho$  based on the global image features and apply this adaptive ratio to the final output visual tokens.

Empirical results of LLaVA-NeXT-8B indicate that FastV+E consistently enhances average performance over the static FastV baseline by 0.3% at energy thresholds of both  $\tau = 99.8\%$  and  $\tau = 99.0\%$ . Specifically, under the  $\tau = 99.8\%$  setting, the adaptive approach improves SQA<sup>I</sup> performance from 73.7 to 74.2. Even with aggressive pruning at  $\tau = 99.0\%$ , E-AdaPrune effectively maintains crucial visual cues, yielding a 0.5 lead in SQA<sup>I</sup> over the static counterpart. Over-



**Fig. 5:** TextVQA visualization ( $\tau = 99.0\%$ ). Compared to static FastV (bottom), FastV+E (middle) adaptively allocates tokens—retaining more for dense scenes to ensure accuracy and fewer for simple scenes to improve efficiency. Green and red indicate correct and incorrect responses, respectively.

all, these results demonstrate that energy-driven adaptive budgeting effectively handles multi-scale visual representations by preserving high-entropy tokens essential for fine-grained reasoning.

Beyond the multi-scale architecture of LLaVA-NeXT, we further evaluate the scalability of E-AdaPrune on LLaVA-1.5-13B to investigate its performance as the LLM capacity increases. Similarly, for LLaVA-1.5-13B, E-AdaPrune consistently outperforms the static FastV baseline at both energy thresholds. At  $\tau = 99.8\%$ , FastV+E improves the average performance from 99.2% to 99.4%, with a notable gain in SQA<sup>I</sup> from 71.3 to 71.9. Under the more aggressive  $\tau = 99.0\%$  setting, the average improvement reaches +0.3%, where SQA<sup>I</sup> shows a significant increase from 72.5 to 73.5. These results demonstrate that the benefit of energy-based adaptive budgeting scales effectively with model size.

#### 4.4 Efficiency and Overhead Analysis

E-AdaPrune (w/ SVD) consistently improves performance under the same average token budget, its overall inference latency remains higher than static baselines. As quantified in Table 3, while total time consumption decreases as the compression ratio  $\rho$  increases, VisionZip+E still incurs a noticeably longer runtime compared to VisionZip. For instance, at a 78% compression ratio, VisionZip requires 628s, whereas VisionZip+E increases to 781s. Since both methods operate under equal effective token counts, this additional latency does not originate from the LLM forward pass, but from the energy estimation procedure itself. In particular, performing a full SVD on the visual feature matrix introduces a non-negligible computational overhead.

To mitigate the computational costs of spectral decomposition, we employ rSVD, as detailed in Appendix Algorithm 2. Table 4 validates the empirical efficiency of this approximation, where we distinguish between Time, representing

**Table 2:** Performance comparison of FastV and FastV+E across different datasets and compression ratios, using LLaVA-NeXT-8B and LLaVA-1.5-13B.

(a) LLaVA-NeXT-8B						(b) LLaVA-1.5-13B					
Method	POPE	SQA <sup>I</sup>	VQA <sup>Text</sup>	GQA	Avg.	Method	POPE	SQA <sup>I</sup>	VQA <sup>Text</sup>	GQA	Avg.
<b>Base</b>	86.6	73.3	65.4	65.4	100%	<b>Base</b>	85.9	71.6	61.3	63.3	100%
$\tau=99.8\%$	1312	679	1292	1320	1151	$\tau=99.8\%$	310	242	295	312	290
FastV	86.4 99.8%	73.7 100.5%	64.8 99.1%	65.2 99.7%	99.8%	FastV	85.2 99.2%	71.3 99.6%	60.8 99.2%	62.6 98.9%	99.2%
FastV+E	86.4 99.8%	74.2 101.2%	65.1 99.5%	65.4 100.0%	100.1%	FastV+E	85.3 99.3%	71.9 100.4%	60.8 99.2%	62.4 98.6%	99.4%
$\tau=99.0\%$	722	289	694	734	610	$\tau=99.0\%$	175	114	159	177	156
FastV	85.9 99.2%	73.4 100.1%	63.3 96.8%	64.6 98.8%	98.7%	FastV	81.5 94.9%	72.5 101.3%	60.2 98.2%	60.5 95.6%	97.5%
FastV+E	85.8 99.1%	73.9 100.8%	63.7 97.4%	64.6 98.8%	99.0%	FastV+E	81.4 94.8%	73.5 102.7%	60.2 98.2%	60.6 95.7%	97.8%

**Table 3:** Efficiency and performance comparison between VisionZip and VisionZip+E under various compressed ratios, using the MMB dataset.

Method	Metric	Compressed Ratio		
		0%	55%	78%
VisionZip	Performance	64.3	64.0	62.2
	Time (s)	933	722	628
VisionZip+E	Performance	64.3	<b>64.1</b>	<b>62.5</b>
	Time (s)	933	843	781

the total cumulative runtime for the dataset, and Latency, which quantifies the specific per-image computational overhead introduced by our energy estimation module.

The transition from exact SVD to rSVD significantly alleviates the estimation bottleneck. While exact SVD introduces a 35ms latency per image, utilizing rSVD with a target dimension of  $t = 300$  and  $q = 2$  power iterations reduces this overhead by 77%, down to 8ms, while maintaining an identical MMB performance of 62.5. Consequently, the total dataset runtime is lowered from 781s to 660s, nearing the 628s required by the static baseline. This demonstrates that the additional latency of E-AdaPrune can be effectively mitigated without compromising accuracy.

We further investigate the impact of the power iteration parameter  $q$  on the stability of the adaptive budget. As shown in Table 4, omitting power iterations ( $q = 0$ ) leads to a significant over-estimation of the average visual token count, particularly as the target dimension  $t$  decreases. For instance, at  $t = 300$ , the average token count spikes from 130 to 156 when  $q$  is reduced from 2 to 0.

**Table 4:** Performance and rSVD efficiency on LLaVA-1.5-7B ( $\tau = 99\%$ ). Latency denotes the additional per-image overhead relative to the VisionZip baseline. Results show that  $t = 300, q = 2$  reduces this overhead from  $35ms$  to  $8ms$  while maintaining accuracy.

Method	Dim $t$	Average Token	Time $s$	Latency $ms$	MMB
<b>Base</b>	-	576	895	-	64.3
VisionZip	-	130	628	-	62.2
SVD	1024	130	781	35	62.5
rSVD ( $q = 2$ )	500	130	701	17	62.5
rSVD ( $q = 1$ )	500	130	687	13	62.5
rSVD ( $q = 0$ )	500	131	695	15	62.4
rSVD ( $q = 2$ )	400	130	702	17	62.5
rSVD ( $q = 1$ )	400	130	678	11	62.5
rSVD ( $q = 0$ )	400	136	685	13	62.8
rSVD ( $q = 2$ )	300	130	660	8	62.5
rSVD ( $q = 1$ )	300	131	679	12	62.4
rSVD ( $q = 0$ )	300	156	658	7	62.8

This phenomenon occurs because the visual feature matrix often exhibits a relatively flat spectral decay. Without power iterations, a single random projection fails to accurately resolve the dominant singular values from the noise or the less significant components of the feature space. This leads to an underestimation of the cumulative energy ratio  $C(k)$  for a given rank, forcing the algorithm to select a larger  $k^*$  to satisfy the energy preservation threshold  $\tau$ . The inclusion of even a single power iteration ( $q = 1$ ) effectively pulls the random subspace toward the dominant singular vectors, ensuring a robust and accurate estimation of the image’s intrinsic energy.

## 5 Conclusion

We presented E-AdaPrune, an energy-driven adaptive visual token pruning framework that determines token budgets from the singular value spectrum of visual features. Unlike static top- $k$  strategies, our method allocates tokens based on input-dependent information density. Experimental results consistently show an average enhancement of up to 0.6%, peaking at a 5.1% relative gain on MMVet. By utilizing rSVD, we reduce the computational overhead to 8ms per image, achieving total runtime comparable to static baselines while maintaining high accuracy.

## References

1. Achiam, J., Adler, S., Agarwal, S., Ahmad, L., Akkaya, I., Aleman, F.L., Almeida, D., Altenschmidt, J., Altman, S., Anadkat, S., et al.: Gpt-4 technical report. arXiv preprint arXiv:2303.08774 (2023)
2. Alayrac, J.B., Donahue, J., Luc, P., Miech, A., Barr, I., Hasson, Y., Lenc, K., Mensch, A., Millican, K., Reynolds, M., et al.: Flamingo: a visual language model for few-shot learning. *Advances in neural information processing systems* **35**, 23716–23736 (2022)
3. Bai, J., Bai, S., Yang, S., Wang, S., Tan, S., Wang, P., Lin, J., Zhou, C., Zhou, J.: Qwen-vl: A versatile vision-language model for understanding, localization, text reading, and beyond. arXiv preprint arXiv:2308.12966 (2023)
4. Bolya, D., Fu, C.Y., Dai, X., Zhang, P., Feichtenhofer, C., Hoffman, J.: Token merging: Your vit but faster. In: *The Eleventh International Conference on Learning Representations* (2023)
5. Cai, M., Yang, J., Gao, J., Lee, Y.J.: Matryoshka multimodal models. In: *The Thirteenth International Conference on Learning Representations* (2025)
6. Cao, J., Ye, P., Li, S., Yu, C., Tang, Y., Lu, J., Chen, T.: Madtp: Multimodal alignment-guided dynamic token pruning for accelerating vision-language transformer. In: *Proceedings of the IEEE/CVF conference on computer vision and pattern recognition*. pp. 15710–15719 (2024)
7. Chen, J., Ye, L., He, J., Wang, Z.Y., Khashabi, D., Yuille, A.: Efficient large multimodal models via visual context compression. *Advances in neural information processing systems* **37**, 73986–74007 (2024)
8. Chen, L., Zhao, H., Liu, T., Bai, S., Lin, J., Zhou, C., Chang, B.: An image is worth 1/2 tokens after layer 2: Plug-and-play inference acceleration for large vision-language models. In: *European Conference on Computer Vision*. pp. 19–35. Springer (2024)
9. Comanici, G., Bieber, E., Schaeckermann, M., Pasupat, I., Sachdeva, N., Dhillon, I., Blistein, M., Ram, O., Zhang, D., Rosen, E., et al.: Gemini 2.5: Pushing the frontier with advanced reasoning, multimodality, long context, and next generation agentic capabilities. arXiv preprint arXiv:2507.06261 (2025)
10. Dai, W., Li, J., Li, D., Tiong, A., Zhao, J., Wang, W., Li, B., Fung, P.N., Hoi, S.: Instructblip: Towards general-purpose vision-language models with instruction tuning. *Advances in neural information processing systems* **36**, 49250–49267 (2023)
11. Du, Z., Qian, Y., Liu, X., Ding, M., Qiu, J., Yang, Z., Tang, J.: Glm: General language model pretraining with autoregressive blank infilling. In: *Proceedings of the 60th Annual Meeting of the Association for Computational Linguistics (Volume 1: Long Papers)*. pp. 320–335 (2022)
12. Fu, C., Chen, P., Shen, Y., Qin, Y., Zhang, M., Lin, X., Yang, J., Zheng, X., Li, K., Sun, X., Wu, Y., Ji, R., Shan, C., He, R.: MME: A comprehensive evaluation benchmark for multimodal large language models. In: *The Thirty-ninth Annual Conference on Neural Information Processing Systems Datasets and Benchmarks Track* (2025)
13. Halko, N., Martinsson, P.G., Tropp, J.A.: Finding structure with randomness: Probabilistic algorithms for constructing approximate matrix decompositions. *SIAM review* **53**(2), 217–288 (2011)
14. Han, Y., Liu, X., Zhang, Z., Ding, P., Wang, D., Chen, H., Yan, Q., Huang, S.: Filter, correlate, compress: Training-free token reduction for mllm acceleration (2025)

15. Hudson, D.A., Manning, C.D.: Gqa: A new dataset for real-world visual reasoning and compositional question answering. In: Proceedings of the IEEE/CVF conference on computer vision and pattern recognition. pp. 6700–6709 (2019)
16. Khaki, S., Guo, J., Tang, J., Yang, S., Chen, Y., Plataniotis, K.N., Lu, Y., Han, S., Liu, Z.: Sparsevila: Decoupling visual sparsity for efficient vlm inference. In: Proceedings of the IEEE/CVF International Conference on Computer Vision (ICCV). pp. 23784–23794 (October 2025)
17. Li, B., Ge, Y., Ge, Y., Wang, G., Wang, R., Zhang, R., Shan, Y.: Seed-bench: Benchmarking multimodal large language models. In: Proceedings of the IEEE/CVF Conference on Computer Vision and Pattern Recognition. pp. 13299–13308 (2024)
18. Li, J., Li, D., Savarese, S., Hoi, S.: Blip-2: Bootstrapping language-image pre-training with frozen image encoders and large language models. In: International conference on machine learning. pp. 19730–19742. PMLR (2023)
19. Li, K., Goyal, S., Semedo, J.D., Kolter, J.Z.: Inference optimal VLMs need fewer visual tokens and more parameters. In: The Thirteenth International Conference on Learning Representations (2025)
20. Li, Y., Du, Y., Zhou, K., Wang, J., Zhao, W.X., Wen, J.R.: Evaluating object hallucination in large vision-language models. In: Proceedings of the 2023 conference on empirical methods in natural language processing. pp. 292–305 (2023)
21. Li, Z., Wu, X., Du, H., Nghiem, H., Shi, G.: Benchmark evaluations, applications, and challenges of large vision language models: A survey. arXiv preprint arXiv:2501.02189 1, 1 (2025)
22. Lin, Z., Lin, M., Lin, L., Ji, R.: Boosting multimodal large language models with visual tokens withdrawal for rapid inference. In: Proceedings of the AAAI Conference on Artificial Intelligence. vol. 39, pp. 5334–5342 (2025)
23. Liu, H., Yan, W., Zaharia, M., Abbeel, P.: World model on million-length video and language with blockwise ringattention. In: The Thirteenth International Conference on Learning Representations (2025)
24. Liu, H., Li, C., Li, Y., Lee, Y.J.: Improved baselines with visual instruction tuning (2024)
25. Liu, H., Li, C., Li, Y., Li, B., Zhang, Y., Shen, S., Lee, Y.J.: Llava-next: Improved reasoning, ocr, and world knowledge (January 2024)
26. Liu, H., Li, C., Wu, Q., Lee, Y.J.: Visual instruction tuning. In: Thirty-seventh Conference on Neural Information Processing Systems (2023)
27. Liu, Y., Duan, H., Zhang, Y., Li, B., Zhang, S., Zhao, W., Yuan, Y., Wang, J., He, C., Liu, Z., et al.: Mmbench: Is your multi-modal model an all-around player? In: European conference on computer vision. pp. 216–233. Springer (2024)
28. Lu, P., Mishra, S., Xia, T., Qiu, L., Chang, K.W., Zhu, S.C., Tafjord, O., Clark, P., Kalyan, A.: Learn to explain: Multimodal reasoning via thought chains for science question answering. *Advances in neural information processing systems* **35**, 2507–2521 (2022)
29. Luo, R., Shan, R., Chen, L., Liu, Z., Wang, L., Yang, M., Xia, X.: VCM: Vision concept modeling with adaptive vision token compression via instruction fine-tuning. In: The Thirty-ninth Annual Conference on Neural Information Processing Systems (2025)
30. Mahoney, M.W.: Randomized algorithms for matrices and data. *Foundations and Trends® in Machine Learning* **3**(2), 123–224 (2011)
31. OpenAI: Gpt-4v(ision) system card (2023)

32. Shang, Y., Cai, M., Xu, B., Lee, Y.J., Yan, Y.: Llava-prumerge: Adaptive token reduction for efficient large multimodal models. In: Proceedings of the IEEE/CVF International Conference on Computer Vision. pp. 22857–22867 (2025)
33. Singh, A., Natarajan, V., Shah, M., Jiang, Y., Chen, X., Batra, D., Parikh, D., Rohrbach, M.: Towards vqa models that can read. In: Proceedings of the IEEE/CVF conference on computer vision and pattern recognition. pp. 8317–8326 (2019)
34. Team, G., Georgiev, P., Lei, V.I., Burnell, R., Bai, L., Gulati, A., Tanzer, G., Vincent, D., Pan, Z., Wang, S., et al.: Gemini 1.5: Unlocking multimodal understanding across millions of tokens of context. arXiv preprint arXiv:2403.05530 (2024)
35. Vaswani, A., Shazeer, N., Parmar, N., Uszkoreit, J., Jones, L., Gomez, A.N., Kaiser, Ł., Polosukhin, I.: Attention is all you need. *Advances in neural information processing systems* **30** (2017)
36. Wang, P., Bai, S., Tan, S., Wang, S., Fan, Z., Bai, J., Chen, K., Liu, X., Wang, J., Ge, W., et al.: Qwen2-vl: Enhancing vision-language model’s perception of the world at any resolution. arXiv preprint arXiv:2409.12191 (2024)
37. Xing, L., Huang, Q., Dong, X., Lu, J., Zhang, P., Zang, Y., Cao, Y., He, C., Wang, J., Wu, F., et al.: Conical visual concentration for efficient large vision-language models. In: Proceedings of the IEEE/CVF Conference on Computer Vision and Pattern Recognition. pp. 14593–14603 (2025)
38. Yang, S., Chen, Y., Tian, Z., Wang, C., Li, J., Yu, B., Jia, J.: Visionzip: Longer is better but not necessary in vision language models. In: Proceedings of the IEEE/CVF Conference on Computer Vision and Pattern Recognition. pp. 19792–19802 (2025)
39. Yang, S., Li, J., Lai, X., Wu, J., Li, W., MA, Z., Yu, B., Zhao, H., Jia, J.: Visionthink: Smart and efficient vision language model via reinforcement learning. In: The Thirty-ninth Annual Conference on Neural Information Processing Systems (2025)
40. Yang, S., Xu, R., Cui, C., Wang, T., Lin, D., Pang, J.: Vflowopt: A token pruning framework for lmms with visual information flow-guided optimization. In: Proceedings of the IEEE/CVF International Conference on Computer Vision. pp. 23924–23934 (2025)
41. Yao, L., Xing, L., Shi, Y., Li, S., Liu, Y., Dong, Y., Zhang, Y.F., Li, L., Dong, Q., Dong, X., et al.: Towards efficient multimodal large language models: A survey on token compression. *Authorea Preprints* (2025)
42. Ye, X., Gan, Y., Ge, Y., Zhang, X.P., Tang, Y.: Atp-llava: Adaptive token pruning for large vision language models. In: Proceedings of the IEEE/CVF Conference on Computer Vision and Pattern Recognition. pp. 24972–24982 (2025)
43. Ye, X., Gan, Y., Huang, X., Ge, Y., Tang, Y.: Voco-llama: Towards vision compression with large language models. In: Proceedings of the Computer Vision and Pattern Recognition Conference. pp. 29836–29846 (2025)
44. Yu, W., Yang, Z., Li, L., Wang, J., Lin, K., Liu, Z., Wang, X., Wang, L.: Mmvet: Evaluating large multimodal models for integrated capabilities. arXiv preprint arXiv:2308.02490 (2023)
45. Zhang, J., Huang, J., Jin, S., Lu, S.: Vision-language models for vision tasks: A survey. *IEEE transactions on pattern analysis and machine intelligence* **46**(8), 5625–5644 (2024)
46. Zhang, P., Dong, X., Wang, B., Cao, Y., Xu, C., Ouyang, L., Zhao, Z., Duan, H., Zhang, S., Ding, S., et al.: Internlm-xcomposer: A vision-language large model for advanced text-image comprehension and composition. arXiv preprint arXiv:2309.15112 (2023)

47. Zhang, Q., Cheng, A., Lu, M., Zhang, R., Zhuo, Z., Cao, J., Guo, S., She, Q., Zhang, S.: Beyond text-visual attention: Exploiting visual cues for effective token pruning in vlms. In: Proceedings of the IEEE/CVF International Conference on Computer Vision. pp. 20857–20867 (2025)
48. Zhang, Y., Fan, C.K., Ma, J., Zheng, W., Huang, T., Cheng, K., Gudovskiy, D.A., Okuno, T., Nakata, Y., Keutzer, K., Zhang, S.: SparseVLM: Visual token sparsification for efficient vision-language model inference. In: Forty-second International Conference on Machine Learning (2025)
49. Zhu, D., Chen, J., Shen, X., Li, X., Elhoseiny, M.: MiniGPT-4: Enhancing vision-language understanding with advanced large language models. In: The Twelfth International Conference on Learning Representations (2024)
50. Zou, X., Lu, D., Wang, Y., Yan, Y., Lyu, Y., Zheng, X., Zhang, L., Hu, X.: Don't just chase "highlighted tokens" in MLLMs: Revisiting visual holistic context retention. In: The Thirty-ninth Annual Conference on Neural Information Processing Systems (2025)

## Appendix

---

### Algorithm 2: Efficient Energy-based Rank Selection via Randomized SVD

---

**Input:** Visual features  $\mathbf{Z}^V \in \mathbb{R}^{n_v \times d_v}$ , Energy threshold  $\tau$ , Target dimension  $k$ ,  
Oversampling  $p$ , Power iteration times  $Q$ , Rank range  $[k_{min}, k_{max}]$

**Output:** Optimal rank  $k^*$ , Dropping ratio  $\rho$

- 1  $E_{total} \leftarrow \|\mathbf{Z}^V\|_F^2 = \sum_{i,j} (z_{i,j}^V)^2$ ; // Reference energy
- // Randomized SVD with Power Iteration
- 2  $k_{sub} \leftarrow \min(t + p, d_v)$ ;
- 3  $\mathbf{\Omega} \leftarrow \text{randn}(d_v, k_{sub})$ ;
- 4  $\mathbf{Y} \leftarrow \mathbf{Z}^V \mathbf{\Omega}$ ;
- 5 **for**  $q = 1$  **to**  $Q$  **do**
- 6  $\mathbf{Y} \leftarrow \mathbf{Z}^V (\mathbf{Z}^{V\top} \mathbf{Y})$ ; // Power iteration for spectral decay
- 7  $\mathbf{Y}, \_ \leftarrow \text{QR}(\mathbf{Y})$
- 8  $\mathbf{B} \leftarrow \mathbf{Y}^\top \mathbf{Z}^V$ ;
- 9  $\tilde{\sigma} \leftarrow \text{SingularValues}(\mathbf{B})$ ;
- // Adaptive Rank Selection
- 10  $k_{raw} \leftarrow \min\{k \mid \frac{\sum_{i=1}^k \tilde{\sigma}_i^2}{E_{total}} \geq \tau\}$ ;
- 11  $k^* \leftarrow \max(k_{min}, \min(k_{raw}, k_{max}))$ ;
- 12  $\rho \leftarrow 1 - k^*/k_{max}$ ;
- 13 **return**  $k^*, \rho$

---